Title

An engineered anti-CA19-9 cys-diabody for positron emission tomography imaging of pancreatic cancer and targeting of polymerized liposomal nanoparticles

Journal

Journal of Surgical Research, 185(1)

ISSN

0022-4804

Authors

Girgis, Mark D
Federman, Noah
Rochefort, Matthew M
et al.

Publication Date

2013-11-01

DOI

10.1016/j.jss.2013.05.095

Peer reviewed

Available online at www.sciencedirect.com

SciVerse ScienceDirect

journal homepage: www.JournalofSurgicalResearch.com

An engineered anti-CA19-9 cys-diabody for positron emission tomography imaging of pancreatic cancer and targeting of polymerized liposomal nanoparticles

Mark D. Girgis, MD,[a,b] Noah Federman, MD,[c] Matthew M. Rochefort, MD,[a,b] Katelyn E. McCabe, PhD,[d] Anna M. Wu, PhD,[d] Jon O. Nagy, PhD,[e] Christopher Denny, MD,[c] and James S. Tomlinson, MD, PhD[a,b,]*

[a] *Department of Surgery, Veterans Healthcare Affairs, Greater Los Angeles, Los Angeles, California*
[b] *Department of Surgery, UCLA, Los Angeles, California*
[c] *Department of Pediatrics, UCLA, Los Angeles, California*
[d] *Crump Institute for Molecular Imaging, Department of Molecular and Medical Pharmacology, UCLA, Los Angeles, California*
[e] *NanoValent Pharmaceuticals, Inc, Bozeman, Montana*

ARTICLE INFO

Article history:
Received 26 April 2013
Received in revised form
26 April 2013
Accepted 24 May 2013
Available online 19 June 2013

Keywords:
Antibody
CA19-9
Imaging
Nanoparticle
Pancreatic cancer

ABSTRACT

Background: Antibody-based therapeutics is a rapidly growing field. Small engineered antibody fragments demonstrate similar antigen affinity compared with the parental antibody but have a shorter serum half-life and possess the ability to be conjugated to nanoparticles. The goal of this study was to engineer an anti-carbohydrate antigen 19-9 (CA19-9) cys-diabody fragment in hopes of targeting nanoparticles to pancreatic cancer.

Methods: The anti-CA19-9 cys-diabody was created by engineering a C-terminal cysteine residue into the DNA single-chain Fv construct of the anti-CA19-9 diabody and expressed in NS0 cells. Maleimide chemistry was used to conjugate the cys-diabody to polymerized liposomal nanoparticles (PLNs) through the cysteine residues. Flow cytometry was used to evaluate targeting of cys-diabody and cys-diabody–PLN conjugate to human pancreatic cancer cell lines. The cys-diabody was radiolabeled with a positron emitter (^{124}I) and evaluated in a mouse model of CA19-9–positive and CA19-9–negative xenografts with micro–positron emission tomography/micro–computed tomography at successive time intervals after injection. Percentage of injected dose per gram of radioactivity was measured in blood and tumor to provide objective confirmation of the micro–positron emission tomographic images.

Results: Tumor xenograft imaging of the anti-CA19-9 cys-diabody demonstrated an average tumor-to-blood ratio of 3.0 and positive-to-negative tumor ratio of 7.4. Successful conjugation of the cys-diabody to PLNs was indicated by flow cytometry showing specific binding of cys-diabody–PLN conjugate to human pancreatic cancer cells *in vitro*.

Conclusions: Our results show that the anti-CA19-9 cys-diabody targets pancreatic cancer providing specific molecular imaging in tumor xenograft models. Furthermore, the cys-diabody–PLN conjugate demonstrates target-specific binding of human pancreatic cancer cells with the potential to deliver targeted treatment.

Published by Elsevier Inc.

* *Corresponding author*. Department of Surgery, UCLA, Los Angeles, CA 90095. Tel.: +1 310 825 2613; fax: +1 310 825 7575.
E-mail address: jtomlinson@mednet.ucla.edu (J.S. Tomlinson).
0022-4804/$ – see front matter Published by Elsevier Inc.
http://dx.doi.org/10.1016/j.jss.2013.05.095

1. Introduction

Cancer is the second most common cause of death among adults [1]. This is often because of late-stage presentation such that metastases are present at diagnosis. Local surgical therapy and chemotherapeutic regimens are variably effective and both are limited by the side effects or morbidity of their uses. Late-stage presentation coupled with ineffective therapy results in inadequate long-term survival. This concept is well illustrated by pancreatic cancer, in which surgery is only partially effective in early-stage patients, chemotherapy is limited by systemic toxicity, and overall survival is approximately 5% [2]. These data indicate the dramatic need for development of novel targeted therapeutics if we are going to improve survival for patients with cancer in all realms of the disease.

One class of targeting agents under intense development is antibodies and engineered antibody fragments (Fig. 1). Antibodies are a unique class of targeting agents capable of exquisite specificity for cell surface antigens. The smallest engineered antibody fragment that retains antigen specificity is the single-chain Fv (scFv) fragment consisting of a variable light chain and a variable heavy chain joined by an amino acid linker [3]. The length of the linker sequence can be adjusted to promote the formation of the diabody, a noncovalent dimer of two scFv fragments [4,5]. The diabody format has been shown to exhibit superior binding affinity and avidity compared with the scFv, likely because of its bivalency for its antigen [6]. Moreover, a covalent dimer of two scFv fragments (cys-diabody) can be created by engineering C-terminal cysteine residues into the DNA construct of the scFv [7]. The cys-diabody has the ability to be site specifically conjugated with fluorophores or radioisotopes through the free sulfhydryl groups of the cysteine residues after reduction of the disulfide bond [7]. The work by Carmichael *et al.* [8] elucidated the crystal structure of the anti-Carcinoembyonic antigen diabody and showed that the C-termini are at the opposite end of the protein's antigen-binding pocket, making it an appealing site to engineer the cysteine residues. This study further suggested that modification in this manner should not alter the diabody's affinity once labeled to a radionuclide through those cysteine residues [8]. The unique ability to conjugate site specifically to these cysteine residues makes the cys-diabody fragment an attractive fragment for therapeutic applications. In particular, it can be used for site-specific conjugation of therapeutic nanoparticles and thus have the potential to deliver targeted therapy to cancer cells.

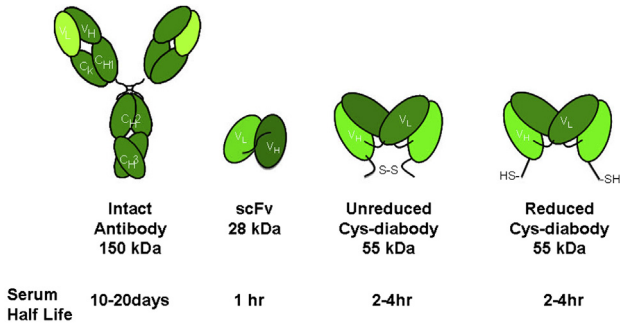

Fig. 1 – Schematic representation of an intact antibody, scFv, unreduced cys-diabody, and reduced cys-diabody. The corresponding half-life and size of the antibody fragments are listed. (Color version of figure is available online.)

Nanoparticles are an emerging class of delivery vehicle for traditional cytotoxic chemotherapeutics with the promise of delivering higher concentrations of chemotherapeutics to the tumor tissue relative to normal tissues [9]. They are easy to prepare in a variety of sizes, are biocompatible, and can carry a wide variety of therapeutics. Additionally, the surfaces of nanoparticles can be easily modified, allowing the potential to perform a myriad of chemical reactions on the nanoparticle surface. Currently, Food and Drug Administration approved that nanoparticles accumulate into tumor tissue through the highly permeable blood vessels of tumors as a result of defective angiogenesis and tend to be retained in tumor tissues because of poor lymphatic drainage. This mechanism known as enhanced permeability and retention guides the accumulation of nanoparticles without necessitating specific tumor targeting [10]. However, this mechanism is still limited by nonspecific uptake into normal tissues. To circumvent this problem and more effectively target nanoparticles to cancer cells minimizing systemic toxicity, nanoparticles have the potential to be chemically conjugated to a tumor-targeting agent, such as the cys-diabody, for antigen-specific localization to tumor cells.

Liposomes in general are one of the most versatile and safe nanoparticles to be applied to cancer chemotherapeutics, owing to their ease of preparation, compatibility with a wide variety of drugs and biomolecules, large carrying capacity, and facile surface coating by targeting or immune system avoidance molecules [11]. An improvement to conventional liposomes is the polymerized liposomal nanoparticles (PLNs) formed from cross-linking polymerized diacetylene lipids. They are of uniform and specified size, are stable, can be reliably produced and modified on the surface (e.g., polyethylene glycol) to render them biocompatible, and can be coated with a tumor-targeting agent. In this regard, they do not elicit an immune response and can target cells, be internalized, and deliver a cytotoxic payload.

Previously, our group evaluated the ability to target the carbohydrate antigen 19-9 (CA19-9) with radiolabeled antibodies in xenograft models of pancreatic cancer [12]. Specifically, we created an anti-CA19-9 diabody that demonstrated good antigen-specific tumor targeting. CA19-9 is a sugar epitope presented on the cell surface proteins of pancreatic cancer cells secondary to aberrant glycosylation of proteins on malignant transformation of epithelial cells. CA19-9 has distinct advantages as a tumor target because of its location on the outermost extent of the cell surface and its abundance. Therefore, the goal of this study was to modify the anti-CA19-9 diabody by engineering cysteine residues into the protein, characterize the newly generated cysteine-modified anti-CA19-9 diabody (anti-CA19-9 cys-diabody), and confirm its ability to retain its targeting potential by itself and while conjugated to PLNs. To do this, we first engineered the

cysteine residues into the C-terminus of the anti-CA19-9 diabody and evaluated its antigen-specific binding ability *in vitro* and *in vivo* using micro–positron emission tomography (micro-PET)/micro–computed tomography (micro-CT). Next, we conjugated the anti-CA19-9 cys-diabody to the surface of the nanoparticle via the free sulfhydryl groups of the reduced cysteine residues. Finally, we evaluated the ability of the anti-CA19-9 cys-diabody–PLN conjugate to discriminate CA19-9–positive cells from negative cells using immunofluorescence studies and flow cytometry.

2. Methods

2.1. Materials

PLNs were obtained from NanoValent Pharmaceuticals, Inc (Bozeman, MT). The lipids comprising the PLNs are *N*-(5′-hydroxy-3′-oxypentyl)-10,12-pentacosadiynoic acid (h-Peg_1-PCDA), *N*-[methoxy(polyethylene glycol)-750]-10,12-pentacosadiynoic acid (m-Peg_{750}-PCDA), *N*-(5′-sulfo-3′-oxypentyl)-10,12-pentacosadiynoic acid (sulfo-Peg_1-PCDA), sodium salt, and *N*-[maleimide(polyethylene glycol)-1500]-10,12-pentacosadiynoic acid (mal-Peg_{1500}-PCDA).

2.2. Construction of the anti-CA19-9 cys-diabody

The scFv DNA fragment in the pUC18 vector (New England Biolabs, Beverly, MA) engineered previously for the anti-CA19-9 diabody was used as the template to perform polymerase chain reaction (PCR) mutagenesis and add the cysteine residues into the C-terminal end of the scFv [13]. This was accomplished using standard PCR components (Invitrogen, Carlsbad, CA) with a 48 bp primer to insert the GGCGG amino acid sequence (5′-GAATTCTCAATGATGATGATGATGATGA CCCCCACACCCACCTGCAGA-3′; IDT Integrated DNA Technologies, San Diego, CA). This construct was confirmed by DNA sequencing, excised from the pUC18 vector, and ligated into the pEE12 mammalian expression vector (Lonza Biologics, Slough, United Kingdom) containing the glutamine synthetase gene for selection and the hCMV promoter for high expression [14].

2.3. Expression, selection, and purification

NS0 murine myeloma cells (5.0×10^6) were transfected by electroporation with 20 μg of linearized pEE12 cys-diabody DNA construct. Cells were selected in glutamine-deficient Dulbecco's Modification of Eagle's Medium (DMEM) or high modified media (JRH Biosciences, Lenexa, KS) as previously described [15,16]. Transfectants were screened for the expression of cys-diabody by Western blot analysis, in which the nitrocellulose membrane (Bio-Rad Laboratories, Hercules, CA) was incubated sequentially with 0.1 μg/mL of anti–penta-His immunoglobulin G (IgG) antibody (Sigma-Aldrich, Bellefonte, PA) and 0.1 μg/mL of alkaline phosphatase (AP)–conjugated goat anti-mouse IgG, Fc-specific antibody (Jackson ImmunoResearch Labs, West Grove, PA) and developed with BCIP/NCP Color Development Substrate (Promega, Madison, WI). Based on the Western blot analysis, high-producing clones were selected for expansion into triple flasks (Nunclon, Rochester, NY). After cell growth and exhaustion in the triple flask stage, the supernatant was harvested and centrifuged to remove cellular debris and then applied onto a 1-mL HiTrap Chelating HP column (GE Healthcare, Piscataway, NJ) at a flow rate of 1 mL/min using an AKTA Purifier (GE Healthcare) for cys-diabody purification. Bound proteins were eluted with 250 mM imidazole in phosphate-buffered saline (PBS). Fractions containing the cys-diabody were evaluated with sodium dodecyl sulfate–polyacrylamide gel electrophoresis (SDS-PAGE), pooled, and dialyzed against PBS using a Slide-A-Lyzer Dialysis Cassette (Thermo Fisher Scientific, Rockford, IL) with a molecular weight cutoff of 10,000 Da to buffer exchange the purified protein. The purified and buffer exchanged cys-diabody was then concentrated using a spin column (Vivaspin 20, 10 kDa cutoff; Thermo Fisher Scientific), and the final cys-diabody protein was stored at 4°C.

2.4. Biochemical characterization of purified anti-CA19-9 cys-diabody protein

The purified anti-CA19-9 cys-diabody was analyzed with SDS-PAGE on precast 4%–20% gels (Bio-Rad Laboratories). Protein samples were incubated with and without the reducing agent, dithiothreitol, at a concentration of 100 mM of dithiothreitol to ensure efficient reduction of the disulfide bond. Gels were stained with Microwave Blue (Protiga Inc, Frederick, MD) for the detection of proteins. Samples were also analyzed with size-exclusion chromatography on a Superdex 75 HR 10/30 column (GE Healthcare). Approximately 50 μg of protein was applied to the column and run isocratically in PBS at a flow rate of 0.5 mL/min on the AKTA Purifier. Elution time was obtained and compared with carbonic anhydrase (30 kDa) and bovine serum albumin (66 kDa) standards (Sigma-Aldrich).

2.5. Cell lines

NS0 mouse myeloma cells were maintained with DMEM or high modified media supplemented with 10% fetal bovine serum (FBS; Invitrogen) and 1% glutamine (Invitrogen). The human pancreatic cancer cell lines, such as BxPC3 and MiaPaca-2 (American Type Culture Collection, Manassas, VA), were maintained in Roswell Park Memorial Insitute-1640 and DMEM, respectively. All media were supplemented with 1% penicillin or streptomycin (Invitrogen) and 10% FBS. Media for the MiaPaca-2 cell line were also supplemented with 2.5% horse serum (Invitrogen) as recommend by the American Type Culture Collection.

2.6. Preparation of PLNs

Liposomes were prepared from h-Peg_1-PCDA, m-Peg_{750}-PCDA, sulfo-Peg_1-PCDA, and mal-Peg_{1500}-PCDA (molar ratio of 6.7:2.6:0.5:0.2) according to the method previously described [17]. Briefly, lipids were mixed and evaporated *in vacuo* to a film. Deionized water was added to the films so as to give a 24 mM (total lipid) suspension. The suspension was heated via sonication between 70°C and 80°C with a probe-tip sonicator (Fisher sonic dismembrator model 300, Fisher Scientific) for 10 min. The resulting clear solution was then cooled to 5°C

for 20 min, warmed to ambient temperature for 20 min, and polymerized by UV light irradiation (254 nm) with a Spectrolinker XL-1000 UV Crosslinker (Spectronics Corp, Lincoln, NE) for 10 min. The resulting blue PLNs were heated to 65°C for 5 min to convert them to the red (fluorescent) form. The colored solutions were syringe filtered through 0.2 μm cellulose acetate filters to remove trace insoluble contaminants. The average particle size measurements were obtained on a Zetasizer Nano-S (Malvern Inst, Worcestershire, UK) in a solution of 10 mM sodium chloride.

2.7. *Conjugation of the anti-CA19-9 cys-diabody to PLNs*

The anti-CA19-9 cys-diabody was conjugated to PLNs using maleimide chemistry. Approximately, 50 μg of cys-diabody in 50 μL of PBS was reduced with 100 μL of immobilized tris (2-carboxyethyl) phosphine (Thermo Fisher Scientific) for 30 min at room temperature. The tris (2-carboxyethyl) phosphine was subsequently spun out of solution in a cellulose spin cup (Thermo Fisher Scientific). The reduced cys-diabody was added immediately to a solution of PLNs (NanoValent Pharmaceuticals, Inc) at a ratio of 50 μg of cys-diabody to 250 μg of PLNs. This mixture was incubated at room temperature for 2 h and dialyzed overnight in PBS buffer using Slide-A-Lyzer Dialysis Cassette (molecular weight cutoff, 100 kDa, Sartorius Stedim Biotech, Goettingen, Germany) to remove any free unbound cys-diabody.

2.8. In vitro *binding assays by flow cytometry and immunofluorescence*

Flow cytometry and immunofluorescence were used to assess the binding ability of both the anti-CA19-9 cys-diabody and the anti-CA19-9 cys-diabody–PLN conjugate. All human pancreatic cell lines were harvested (1×10^6 cells), resuspended in 250 μL of PBS with 2% FBS, and incubated with 4 μg of cys-diabody on ice for 1 h. The cells were washed for 10 min by centrifugation at $1000 \times g$, the supernatant was discarded, and the cells were resuspended in another 250 μL of PBS with 2% FBS. The cells were again incubated with secondary antibody, 4 μg of anti–penta-His IgG antibody (Sigma-Aldrich), for 1 h on ice. Another wash was performed, and the cells were finally incubated for 1 h on ice with 4 μg of tertiary antibody, R-phycoerythrin–conjugated goat anti-mouse IgG, Fc-specific antibody (Jackson Immunoresearch Labs). A final wash was performed, and the cells were resuspended with 500 μL PBS with 2% FBS. Binding data were obtained using a ScanX flow cytometer (Becton Dickinson, Franklin Lakes, NJ) and analyzed using FlowJo software (Tree Star Inc, Ashland, OR).

Similarly, immunofluorescence was performed using six-well plates (Becton Dickinson) with sequential incubation steps of the anti-CA19-9 cys-diabody, secondary antibody, and tertiary antibody with wash steps in between incubations. On completion of all steps, the wells were visualized with a Nikon 90S fluorescent microscope (Nikon Inc, Melville, NY), and images were taken with a 5.1 megapixel CCD camera (Nikon). Fluorescent images were generated with a white light X-Cite 120Q source (Scientifica, East Sussex, UK), using an excitation wavelength bandpass filter of 545–565 nm and an emission wavelength bandpass filter of 580–620 nm. All images were obtained using a magnification lens of 20×. Images were analyzed using Nikon software and were processed for contrast and brightness using Photoshop Elements 4 (Adobe Systems Inc, San Jose, CA).

For both flow cytometry and immunofluorescence, negative control samples included those with cells only or cells incubated with the secondary and tertiary antibodies and no primary antibody. Experimental samples included those with cells incubated with the cys-diabody, secondary, and tertiary antibodies. The positive control samples included those with cells incubated with the parental intact monoclonal antibody (mAb) and tertiary antibody.

Additionally, flow cytometry and immunofluorescence were performed in the same manner using the anti-CA19-9 cys-diabody–PLN conjugate as the primary antibody. Because the PLN exhibits autofluorescence within the same wavelength excitation and emission range as R-phycoerythrin, no secondary and tertiary antibodies were used. Experiments included cells only, cells incubated with cys-diabody–PLN conjugate, and cells incubated with PLNs only as a negative control.

2.9. *Cell-based competition enzyme-linked immunosorbent assay*

To determine the relative binding affinity of the anti-CA19-9 cys-diabody, a cell-based competition enzyme-linked immunosorbent assay was performed. CA19-9–positive cells, BxPC3, were harvested, counted, and aliquoted into a 96-well plate (50,000 cells per well) for adhesion overnight. The following day, the cell media were removed, and each well was washed with 150 μL of PBS and 2% FBS. The wash was also removed, and each well was incubated for 1 h at room temperature with 150 μL of a 1 nM concentration of the parental intact anti-CA19-9 mAb obtained from purifying the supernatant of the 116-N-19-9 hybridoma cells known to produce the mAb [18]. After incubation, the wells were washed similarly and incubated for 1 h at room temperature with 150 μL of varying concentrations, ranging from 0.01 to 100 nM, of the anti-CA19-9 cys-diabody. Again, the wells were washed and incubated with 150 μL of a 1:2500 μL dilution of AP-conjugated goat anti-mouse IgG, Fc-specific antibody (Jackson Immunoresearch Labs). After 1 h, the wells were washed again and developed with 150 μL of a solution of 10 mg phosphatase tabs (Sigma-Aldrich) dissolved in 10 mL of AP buffer. The reaction was permitted to proceed for 15 min and then evaluated for absorbance at 405 nm using the GENios microplate reader (Tecan, Durham, NC). All experiments were done in triplicate. A saturation binding plot was created based on the absorbance value of each sample to calculate the dissociation constant (K_d), defined as the amount of cys-diabody needed to displace 50% of the parental intact anti-CA19-9 mAb.

2.10. *Radioiodination*

Radiolabeling of the anti-CA19-9 cys-diabody with the positron-emitting isotope, iodine-124 (^{124}I), was performed using the iodogen method as described [19] using Pierce Pre-

Coated Iodination Tubes (Thermo Fisher Scientific). The labeling reaction was performed with 200 μg of purified cys-diabody (200 μL) and 800 μCi of $Na^{124}I$ (IBA Molecular, Dulles, VA). Instant thin layer chromatography using the Tec-Control kit (Biodex Medical Systems, Shirley, NY) was used to measure labeling efficiency. Immunoreactivity, defined as the fraction of cys-diabody retaining the ability to bind to cells after radiolabeling, was determined by incubating the radioiodinated cys-diabody (≈100,000 cpm) with BxPC3 and MiaPaca-2 cells in 1 mL of PBS and 2% FBS such that there was an excess of antigen for the positive cell line. The radioiodinated cys-diabody was allowed to incubate with the cells for 1 h at room temperature, after which the cells were centrifuged at 800 *g* for 5 min. The supernatant was removed and collected; the cell pellet was then resuspended in 1 mL of PBS and 2% FBS and collected. The radioactivity in the supernatant and cell pellet was measured in a Wizard 3′ 1480 Automatic Gamma Counter (Perkin-Elmer, Covina, CA). The radioactivity in the cell pellet (bound cys-diabody) was divided by the total radioactivity in the cell pellet plus the supernatant (unbound cys-diabody), yielding the fraction of bound cys-diabody. This fraction was multiplied by 100 yielding the percentage of immunoreactivity.

2.11. *Xenograft imaging and biodistribution studies*

Animal handling was carried out under a protocol approved by the Chancellor's Animal Research Committee of the University of California in Los Angeles (UCLA). The antigen-positive (BxPC3) xenograft models were established with 1×10^6 cells injected subcutaneously into the left shoulder of four female nude mice (Charles River Laboratories, Wilmigton, MA). In the same four mice, the antigen-negative cell line (MiaPaca-2) was injected in the right shoulder as a negative control. Tumors were allowed to develop for approximately 3 wk. Gastric lavage was performed with 1.5 mg of potassium perchlorate in 200 μL of PBS at 30 min before tail vein injection of ^{124}I-anti-CA19-9 cys-diabody. Additionally, blocking of thyroid uptake of radioiodine was accomplished by adding saturated potassium iodide (0.5 mL/100 mL of water) to the drinking water 24 h before injection of the radioiodinated cys-diabody. Mice were injected with approximately 25 μg of ^{124}I-anti-CA19-9 cys-diabody (specific activity of 4.03 ± 1.8 μCi/μg) in PBS and 2% FBS via the tail vein. Micro-PET was performed at 4 and 20 h after injection. These time points for imaging were chosen based on previously measured half-lives of diabody fragments and corresponded to approximately one half-life and five half-lives, respectively [7,20,21]. Also, to appropriately compare the *in vivo* targeting ability of the anti-CA19-9 cys-diabody to the anti-CA19-9 diabody, we performed the imaging experiments at the same time points as previously published for the anti-CA19-9 diabody [12]. The mice were anesthetized using 2% isoflurane, placed on the micro-PET bed, and imaged with a Focus micro-PET scanner (Concorde Microsystems Inc, Knoxville, TN). Acquisition time was 10 min. All images were reconstructed using a FBP algorithm and displayed by the AMIDE software package [22,23]. One mouse was subsequently imaged with micro-CT, and the micro-CT images were coregistered with the micro-PET images to provide an anatomic reference. Animals were euthanized after the last imaging time point, and organs, tumors, and blood were harvested and weighed. Radioactive uptake of organs was counted in a gamma counter for biodistribution analysis and converted to a percentage of injected doses of radioactivity per gram of tissue after decay correction.

3. Results

3.1. *Construction of the anti-CA19-9 cys-diabody*

Using the anti-CA19-9 diabody DNA as a template, PCR mutagenesis was performed to insert the C-terminal cysteine residues. Gene sequencing and comparison with the published sequence confirmed success [24].

3.2. *Expression, selection, and purification*

The cys-diabody was expressed in NS0 myeloma cells. Cell culture supernatant was harvested and analyzed with Western blot analysis to determine those clones expressing the highest levels of protein. These were selected for expansion into triple flasks (Nunclon). Selected clone expression ranged from 10 to 45 mg/L. The 6×His tag engineered on the C-terminus of the anti-CA19-9 cys-diabody was used for protein purification. Approximately 100 mL of the culture supernatant yielded 1–4.5 mg of pure protein.

3.3. *Biochemical characterization of the anti-CA19-9 cys-diabody*

The protein purity of the isolated cys-diabody obtained from metal affinity chromatography was confirmed by SDS-PAGE and Western blot analysis (Fig. 2A and B). Size-exclusion chromatography was done to evaluate for the presence of the appropriate covalent interactions between two scFv fragments to form the cys-diabody (Fig. 2C). As shown, compared with bovine serum albumin (20.75 min) and carbonic anhydrase (24.75 min) standards, the cys-diabody elution time was 23.98 min. The elution time of the cys-diabody was consistent with its predicted molecular weight of 55 kDa.

3.4. In vitro *binding assays for the characterization of the anti-CA19-9 cys-diabody*

CA19-9 recognition and binding were evaluated by flow cytometry and immunofluorescence. The anti-CA19-9 cys-diabody demonstrated the ability to distinguish between the CA19-9–positive cell line, BxPC3, and the CA19-9–negative cell line, MiaPaca-2, by flow cytometry (Fig. 3A). The cys-diabody exhibited slightly lower binding efficiency compared with the parental intact anti-CA19-9 antibody. MiaPaca-2 showed no expression of CA19-9 and served as the negative control. Immunofluorescence data were in accordance with the flow cytometry data (Fig. 3B). The MiaPaca-2 cell line showed no binding of the cys-diabody, whereas the BxPC3 cell line showed binding of the cys-diabody to the cells *in vitro*.

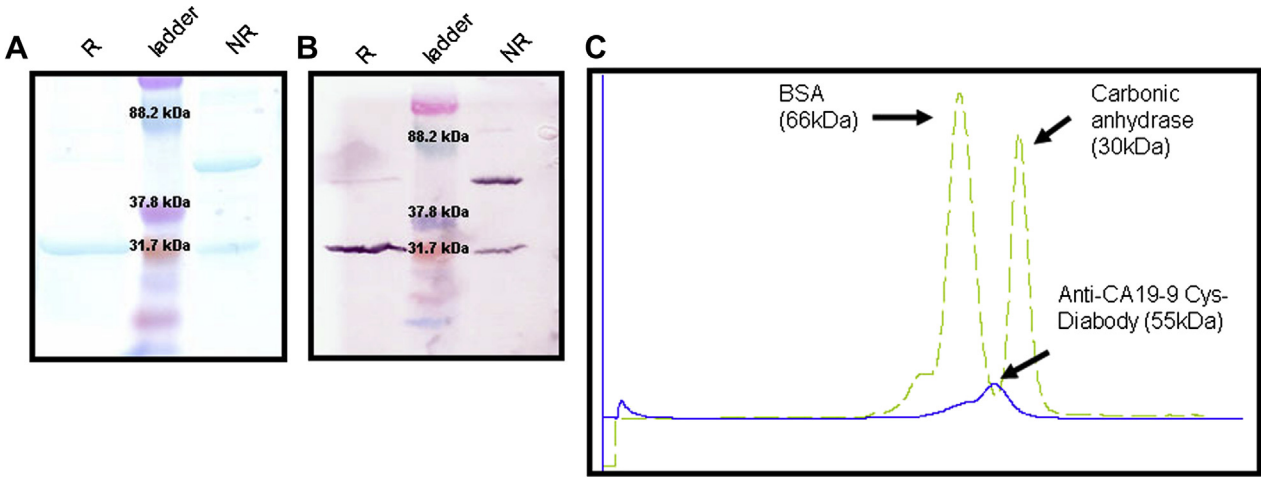

Fig. 2 – *In vitro* biochemical characterization of the anti-CA19-9 cys-diabody. (A) SDS-PAGE of purified anti-CA19-9 cys-diabody. (B) Western blot of purified anti-CA19-9 cys-diabody. R is reduced and NR is nonreduced. (C) Size-exclusion chromatography elution profile of the anti-CA19-9 cys-diabody in relation to the known standards of BSA (66 kDa) and carbonic anhydrase (30 kDa). The diabody eluted at 22.98 min after injection into the column as expected for a 55 kDa diabody. BSA = bovine serum albumin. (Color version of figure is available online.)

3.5. *Cell-based competition enzyme-linked immunosorbent assay*

A competition binding assay as described was performed to ascertain the relative binding affinity of the anti-CA19-9 cys-diabody compared with the murine anti-CA19-9 intact antibody. The absorbance values obtained for each sample were averaged and plotted on a saturated binding plot. The observed relative binding affinity of the diabody was approximately 6 nM (Fig. 3C).

3.6. *Radioiodination, xenograft imaging, and biodistribution studies*

In vivo tumor targeting of the anti-CA19-9 cys-diabody was evaluated with micro-PET imaging. Nude mice carrying CA19-9–positive (BxPC3) and CA19-9–negative (MiaPaca-2) tumors were injected with the ^{124}I-labeled anti-CA19-9 cys-diabody. The labeling efficiency of ^{124}I on the anti-CA19-9 cys-diabody was 96%. Immunoreactivity of the ^{124}I-labeled anti-CA19-9 cys-diabody on BxPC3 and MiaPaca-2 cells was 75% and 1%, respectively. Micro-PET imaging studies were conducted in four animals bearing BxPC3 tumors averaging 36 mg (range, 9–67 mg) and MiaPaca-2 tumors averaging 29 mg (range, 21–39 mg) and obtained at 4 and 20 h after injection of the cys-diabody. Figure 4 illustrates representative images from each study. After the 20-h time point, all four mice were sacrificed and organs were harvested for measurement of radioactivity to provide quantitative evidence of tumor targeting. These data were used to calculate tumor-to-blood ratios in each animal. For the four mice bearing BxPC3 tumors, the positive tumor activity averaged 1.1% ID/g with a range of 0.4–1.7% ID/g. The average negative tumor activity in this model was 0.2% ID/g (range, 0.1–0.3% ID/g). The difference in percentage of injected doses of radioactivity per gram between the positive tumor and the blood trended toward but did not reach significance ($P = 0.077$); however, the difference between the positive and the negative tumors ($P = 0.043$) was able to reach significance as determined by paired *t*-test. The average tumor-to-blood ratio was 2.7:1, and the positive-to-negative tumor ratio was 6:1. High uptake was noted in the liver (data not shown).

3.7. *Construction of maleimide PLNs and characterization*

PLNs were synthesized by the self-assembly of lipids into small unilamellar liposomes. The polymerizable lipids contain diacetylene groups in the fatty acid tails. Methoxy- and maleimide-terminated polyethylene glycol polymers are appended to the liposome-forming lipids by chemically conjugating them to the carboxyl groups in the commercially available pentacosadiynoic acid lipid (GFS Chemicals, Powell, OH). Aqueous dispersions of the lipids are sonicated while being heated to a temperature above the lipid phase transition giving liposomes that appear as clear solutions. To obtain PLNs (polydiacetylene), the lipid chains must be in a tightly packed solid analogous state as part of the membrane bilayer [25]. This is achieved by cooling the liposome solution to 5°C for 20 min. After warming, the solutions are irradiated with UV light to initiate a radical polymerization process, resulting in a deeply blue–purple colored PLN solution.

The blue–purple form of the PLN is only slightly fluorescent, and to obtain highly fluorescent particles, the solutions are briefly heated. This results in a slight perturbation of the polydiacetylene polymer backbone that results in a chromatic shift in color and fluorescence [26,27]. The fluorescence emission spectrum is centered at 635 nm with a broad and

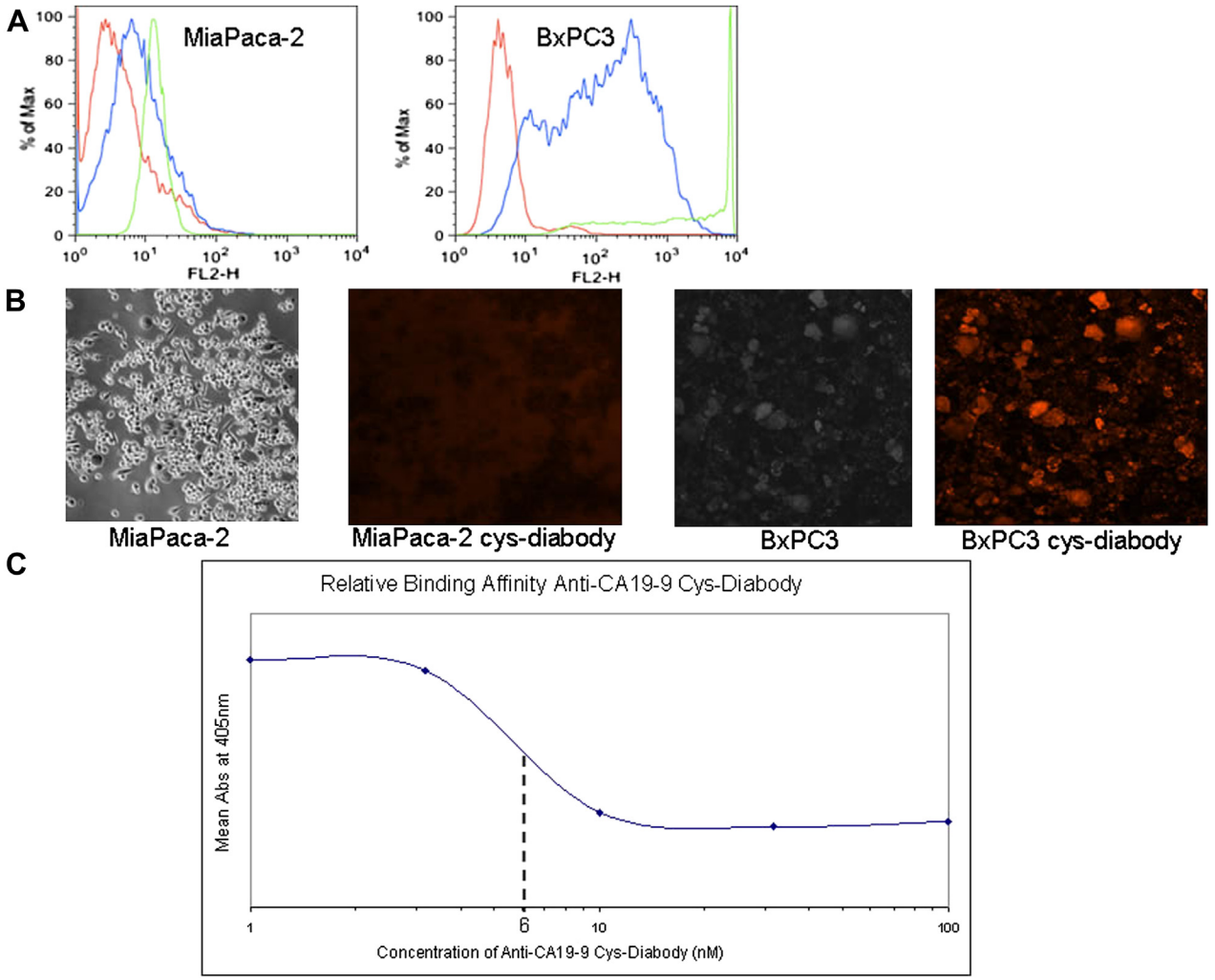

Fig. 3 – *In vitro* functional characterization of the anti-CA19-9 cys-diabody. (A) Flow cytometry showing binding specificity of the anti-CA19-9 cys-diabody to each cell line. Red line shows cells incubated with only mouse anti–penta-His antibody and phycoerythrin-conjugated goat anti-mouse antibody. Green line shows cells incubated with commercial intact mouse anti-CA19-9 antibody and phycoerythrin-conjugated goat anti-mouse antibody. Blue line shows cells incubated with anti-CA19-9 cys-diabody, mouse anti–penta-His antibody, and phycoerythrin-conjugated goat anti-mouse antibody. (B) Immunofluorescence showing binding specificity of anti-CA19-9 cys-diabody. Cells were incubated with anti-CA19-9 cys-diabody, mouse anti–penta-His antibody, and phycoerythrin-conjugated goat anti-mouse antibody. (C) Relative binding affinity of the anti-CA19-9 cys-diabody compared with the parental intact antibody. (Color version of figure is available online.)

complex excitation spectrum from 480 to 580 nm. We have seen some evidence that cellular uptake of the nonfluorescing PLNs rapidly converts them into fluorescent form (unpublished data). For the cell uptake studies, however, we preheated the PLNs to convert them all into their fluorescent form. A distinct advantage to the PLN fluorescence is that little or no photobleaching occurs.

The PLNs resulting from simple probe-tip sonication of this lipid formulation give a fairly tight population of small-sized particles. Particle size analysis shows them to be typically in a size range from 30 to 50 nm, with the average size centering around 38 nm. No attempts were made to produce tighter size ranges by membrane extrusion, although this technique is applicable to the liposome preparation step and will be conducted for material that will subsequently be administered *in vivo* in future studies.

3.8. *Conjugation of the anti-CA19-9 cys-diabody to PLNs*

Approximately 200 μg of anti-CA19-9 cys-diabody was used for conjugation to 1000 μg of PLNs (Fig. 5). The reaction time was 2 h. Reaction efficiency was approximately 80% measured by calculation of the amount of cys-diabody remaining after buffer exchange. Additionally, this conjugation reaction demonstrated storage stability at 4°C as all experiments were duplicated 1 mo after conjugation with similar results.

3.9. *In vitro binding assays for characterization of the anti-CA19-9 cys-diabody–PLN conjugate*

Flow cytometry of the anti-CA19-9 cys-diabody–PLN conjugate displayed similar results compared with that of the

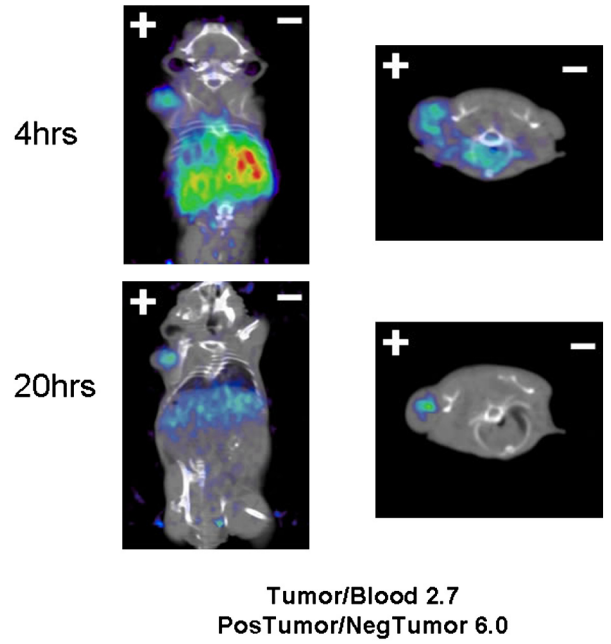

Fig. 4 – *In vivo* micro-PET and micro-CT images of BxPC3 xenografts at 4 and 20 h with those associated tumor-to-blood ratios and positive-to-negative tumor ratios obtained after the 20-h image. (Color version of figure is available online.)

unconjugated anti-CA19-9 cys-diabody (Fig. 6). The fluorescent nature of the PLN allowed the cys-diabody–PLN conjugate to discriminate between the positive and the negative cell lines by both immunofluorescence and flow cytometry. The lack of a fluorescent secondary antibody confirms that the cys-diabody–PLN conjugation is the only source of fluorescence; therefore, the presence and localization of the fluorescent PLN demonstrate continued conjugation of the PLN to the antigen-specific cys-diabody. Furthermore, immunofluorescence of the cys-diabody–PLN conjugate demonstrated a pattern of localization to the outer surface of the cell membrane (Fig. 6).

4. Discussion

Previously, we investigated the potential of an anti-CA19-9 diabody to target pancreatic cancer xenografts in a mouse model [12]. CA19-9 was chosen because of its prevalence on >90% of all pancreatic cancers and its accessibility on the outer surface of cell membranes [28–31]. In addition to its widespread prevalence and accessibility, it is very abundant with expression estimated to be between 1 and 2 million antigens per cell. Based on these attributes, it represents an ideal tumor target. With the anti-CA19-9 diabody, we were able to demonstrate targeting of CA19-9 *in vitro* and *in vivo* [12]. These results encouraged us to modify the diabody to a cys-diabody and exploit the unique ability to site specifically conjugate to this fragment. To this end, we engineered, produced, and characterized the anti-CA19-9 cys-diabody. We show that our cys-diabody exhibits similar biochemical properties to other engineered cys-diabodies, displaying a molecular weight of 55 kDa and forming a covalent dimer [7,13]. In addition, we demonstrate specific binding of CA19-9 with the cys-diabody by flow cytometry and immunofluorescence with similar binding affinity compared with the parental anti-CA19-9 diabody.

To ensure that the modification of C-terminal cysteine residues did not alter the *in vivo* binding properties of the diabody, we investigated the ability of the cys-diabody to target CA19-9 by injecting mice harboring the BxPC3 and MiaPaca-2 xenografts via the tail vein with ^{124}I-labeled anti-CA19-9 cys-diabody. Micro-PET images at 4 h demonstrated quick targeting of the antibody fragment to the BxPC3 xenograft (CA19-9 positive), similar to the parental anti-CA19-9 diabody. Additionally, we showed that the cys-diabody was retained at the site of the xenograft based on the persistence of signal on micro-PET images at the 20-h time point. Biodistribution data, corrected for time of injection, provided raw numerical values expressed in percentage of the injected doses of radioactivity per gram of tissue and was ascertained for the positive tumors, negative tumors, blood, and organs. The positive tumors demonstrated an average of 1.1% ID/g

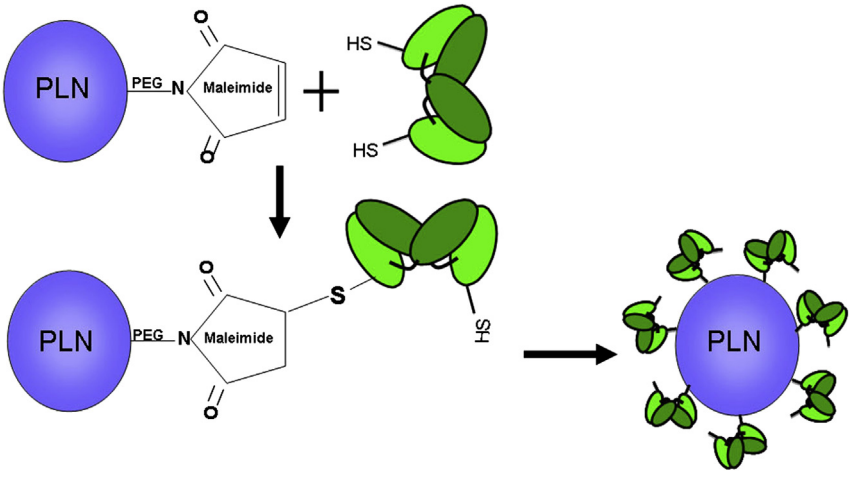

Fig. 5 – Conjugation reaction between the PLN and the cys-diabody. The cys-diabody is reduced to create free sulfhydryl groups that are then used to covalently link through the maleimide group to the PLN. (Color version of figure is available online.)

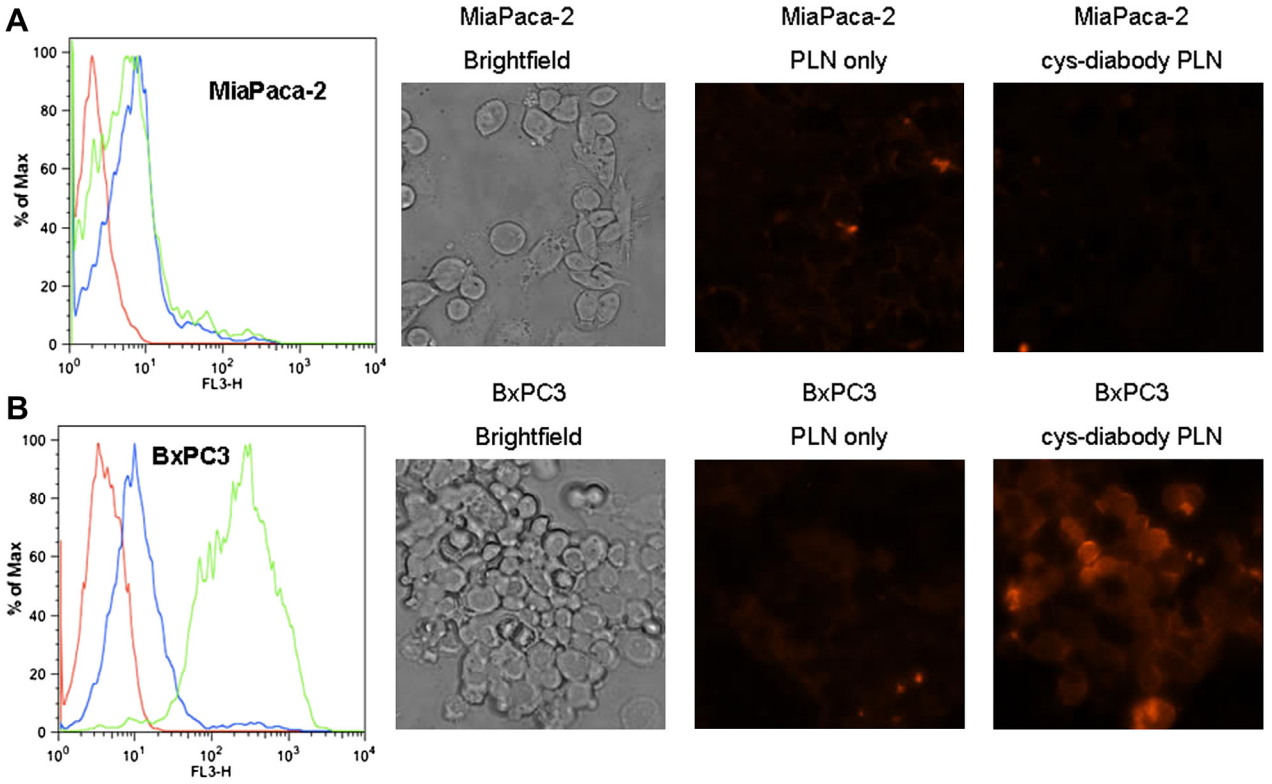

Fig. 6 – *In vitro* characterization of the anti-CA19-9 cys-diabody–PLN conjugate. (A) Flow cytometry and immunofluorescence using MiaPaca-2 cells. (B) Flow cytometry and immunofluorescence using BxPC3 cells. Note in (A) and (B): red line shows cells only; blue line shows cells incubated with PLN only; and green line shows cells incubated with anti-CA19-9 cys-diabody–PLN conjugate. (Color version of figure is available online.)

and a positive tumor-to-blood ratio of 2.7:1, which is consistent with the parental anti-CA19-9 diabody values of 1.1% ID/g and ratio of 5:1 previously published by our group [12]. As expected, the liver demonstrated a high percentage of injected doses of radioactivity per gram accounting for the presence of signal in the liver on micro-PET images. This phenomenon is explained best by Ahlgren *et al.* [32] who characterized a Her2 affibody with and without a 6×His tag noting that the affibody with the 6×His tag had significantly increased amount of liver uptake compared with the Her2 affibody without the tag. Although this phenomenon has not been specifically described in humans, it represents a potential obstacle to clinical translation of proteins engineered with 6×His tags and can be overcome with alternate purification techniques not requiring the 6×His tag. More importantly, a tumor-to-blood ratio of 2.7:1 and a positive-to-negative tumor ratio of 6:1 were obtained. These values indicate that the images display enough contrast between the tumor and the blood (i.e., background) to be visualized. Not only do these data indicate antigen-specific targeting of the BxPC3 xenograft but also provide evidence of the potential of the anti-CA19-9 cys-diabody as a targeting agent for pancreatic cancer.

After confirming the cys-diabody's ability to antigen specifically target CA19-9–positive cells both *in vitro* and *in vivo*, we set out to develop a site-specific conjugation reaction to add our anti-CA19-9 cys-diabody to the surface of our PLNs. By reducing the disulfide bonds of the C-terminal cysteine residues, free sulfhydryl groups are available for conjugation to PLNs using maleimide chemistry. The maleimide group was incorporated onto the PLN surface right from the assembly stage by attaching it to one of the PLN-forming lipids. To confirm that the cys-diabody–PLN conjugate was created and that it bound to cells in an antigen-specific manner, we conducted a number of studies. Given the PLN's inherent autofluorescence, we assumed that a cell with PLN bound would be captured by the flow cytometry detector without any additional method of detection [33]. The negative cell line showed no fluorescence with the PLN alone or with the conjugate solution, and the BxPC3 cells demonstrated fluorescence only with the cys-diabody–PLN conjugate and not with the PLN alone. These results confirm that the conjugation reaction was successful and that we are able to target PLNs to cancer cells *in vitro* through the specific antibody–antigen interaction of the anti-CA19-9 cys-diabody.

This achievement further defines the potential to deliver targeted treatment to cancer cells. By virtue of the ability of PLNs to serve as vehicles for chemotherapeutic agents, this could provide a method by which our targeting agent, the anti-CA19-9 cys-diabody, can be applied for delivery of targeted therapy. Although further studies evaluating the ability of the cys-diabody–PLN conjugate to target pancreatic cancer and other cancers *in vivo* need to be performed, the potential for an

antigen-specific technique for delivery of chemotherapeutics is promising.

5. Conclusions

Diabodies are small bivalent antibody fragments that are highly specific agents that can be used to target tumor antigens. In this study, we expand on our previous results with the anti-CA19-9 diabody by engineering the anti-CA19-9 cys-diabody to exploit its ability to be site specifically conjugated to PLNs. After modifying the diabody to the cys-diabody, we show that the antibody fragment retains its antigen specificity *in vitro* and *in vivo* providing antigen-specific micro-PET imaging of pancreatic cancer xenografts in a mouse model. Additionally, we demonstrated that the cys-diabody can be covalently conjugated to PLNs while retaining its immunoreactivity against the tumor antigen CA19-9. This report using site-specific conjugation of a cys-diabody to a nanoparticle opens the door to a wide variety of possible therapeutic and diagnostic applications because of the flexible nature of these liposomal vehicles. Passive targeting via the enhanced permeability and retention effect may not be sufficient to create a significant treatment advantage at the tumor compared with the normal tissues. By creating an anti-CA19-9-PLN immunoconjugate, we can achieve "active targeting" through antibody–antigen recognition, which may improve our tumor-specific delivery of therapeutic agents and minimize the bystander effects to normal cells from these cytotoxins. In such a way, we have the potential to deliver a cytotoxic payload to cancer cells in an antigen-specific manner.

Acknowledgment

This work was supported by the Veterans Affairs Career Development Award (J.S.T.). The authors thank Waldemar Ladno for his assistance with the animal studies and Felix Bergara, MS, for his technical assistance. They also acknowledge the UCLA Translation Pathology Core Laboratory for their immunostaining services and the UCLA Small Animal Imaging Resource Program (NIH CA 92865). Flow cytometry was performed in the UCLA Jonsson Comprehensive Cancer Center and Center for AIDS Research Flow Cytometry Core Facility, supported by NIH awards (CA-16042 and AI-28697).

Authors contributions: M.D.G. carried out the antibody production and evaluation and drafted the manuscript. N.F., C.D., and J.O.N. participated in drafting the manuscript and study design. K.E.M. carried out antibody evaluation and conjugation to nanoparticles. M.M.R. contributed to manuscript preparation. A.M.W. contributed to study design and manuscript preparation. J.S.T. conceived of the study, participated in its design and coordination, and helped to draft the manuscript. All the authors read and approved the final manuscript.

Competing interests: The authors have one competing interest to report. Dr J.O.N. is the owner of NanoValent Pharmaceuticals Inc, where the PLN is constructed. Dr A.M.W is a shareholder in ImaginAb Inc, which has licensed some of the technology described in this article.

REFERENCES

[1] American Cancer Society. Cancer facts & figures. Atlanta (GA): American Cancer Society; 2011.
[2] Wasif N, Ko CY, Farrell J, et al. Impact of tumor grade on prognosis in pancreatic cancer: should we include grade in AJCC staging? Ann Surg Oncol 2010;17:2312.
[3] Kenanova V, Wu AM. Tailoring antibodies for radionuclide delivery. Expert Opin Drug Deliv 2006;3:53.
[4] Kortt AA, Dolezal O, Power BE, Hudson PJ. Dimeric and trimeric antibodies: high avidity scFvs for cancer targeting. Biomol Eng 2001;18:95.
[5] Holliger P, Prospero T, Winter G. "Diabodies": small bivalent and bispecific antibody fragments. Proc Natl Acad Sci U S A 1993;90:6444.
[6] Adams GP, Tai MS, McCartney JE, et al. Avidity-mediated enhancement of in vivo tumor targeting by single-chain Fv dimers. Clin Cancer Res 2006;12:1599.
[7] Olafsen T, Cheung CW, Yazaki PJ, et al. Covalent disulfide-linked anti-CEA diabody allows site-specific conjugation and radiolabeling for tumor targeting applications. Protein Eng Des Sel 2004;17:21.
[8] Carmichael JA, Power BE, Garrett TP, et al. The crystal structure of an anti-CEA scFv diabody assembled from T84.66 scFvs in V(L)-to-V(H) orientation: implications for diabody flexibility. J Mol Biol 2003;326:341.
[9] Weinberg BD, Ai H, Blanco E, Anderson JM, Gao J. Antitumor efficacy and local distribution of doxorubicin via intratumoral delivery from polymer millirods. J Biomed Mater Res A 2007;81:161.
[10] Brannon-Peppas L, Blanchette JO. Nanoparticle and targeted systems for cancer therapy. Adv Drug Deliv Rev 2004;56:1649.
[11] Federman N, Denny CT. Targeting liposomes toward novel pediatric anticancer therapeutics. Pediatr Res 2010;67:514.
[12] Girgis MD, Kenanova V, Olafsen T, McCabe KE, Wu AM, Tomlinson JS. Anti-CA19-9 diabody as a PET imaging probe for pancreas cancer. J Surg Res 2011;170:169.
[13] Sirk SJ, Olafsen T, Barat B, Bauer KB, Wu AM. Site-specific, thiol-mediated conjugation of fluorescent probes to cysteine-modified diabodies targeting CD20 or HER2. Bioconjug Chem 2008;19:2527.
[14] Bebbington CR, Renner G, Thomson S, et al. High-level expression of a recombinant antibody from myeloma cells using a glutamine synthetase gene as an amplifiable selectable marker. Biotechnology (N Y) 1992;10:169.
[15] Galfre G, Milstein C. Preparation of monoclonal antibodies: strategies and procedures. Methods Enzymol 1981;73:3.
[16] Kenanova V, Olafsen T, Crow DM, et al. Tailoring the pharmacokinetics and positron emission tomography imaging properties of anti-carcinoembryonic antigen single-chain Fv-Fc antibody fragments. Cancer Res 2005; 65:622.
[17] Bruehl RE, Dasgupta F, Katsumoto TR, et al. Polymerized liposome assemblies: bifunctional macromolecular selectin inhibitors mimicking physiological selectin ligands. Biochemistry 2001;40:5964.
[18] Koprowski H, Steplewski Z, Mitchell K, et al. Colorectal carcinoma antigens detected by hybridoma antibodies. Somatic Cell Genet 1979;5:957.
[19] Markwell MA, Fox CF. Surface-specific iodination of membrane proteins of viruses and eucaryotic cells using 1,3,4,6-tetrachloro-3alpha,6alpha-diphenylglycoluril. Biochemistry 1978;17:4807.
[20] McCartney JE, Tai MS, Hudziak RM, et al. Engineering disulfide-linked single-chain Fv dimers [(sFv')2] with improved solution and targeting properties: anti-digoxin

26-10 (sFv')2 and anti-c-erbB-2 741F8 (sFv')2 made by protein folding and bonded through C-terminal cysteinyl peptides. Protein Eng 1995;8:301.
[21] Williams LE, Wu AM, Yazaki PJ, et al. Numerical selection of optimal tumor imaging agents with application to engineered antibodies. Cancer Biother Radiopharm 2001; 16:25.
[22] Defrise M, Kinahan PE, Townsend DW, et al. Exact and approximate rebinning algorithms for 3-D PET data. IEEE Trans Med Imaging 1997;16:145.
[23] Loening AM, Gambhir SS. AMIDE: a free software tool for multimodality medical image analysis. Mol Imaging 2003; 2:131.
[24] Tonge DW, Hennam JF, Greene AR, Lee ID, Edge MD. Cloning and characterization of 1116NS19.9 heavy and light chain cDNAs and expression of antibody fragments in Escherichia coli. Year Immunol 1993;7:56.
[25] Day D, Ringsdorf H. Polymerization of diacetylene carbonic-acid monolayers at gas-water interface. J Polym Sci Pol Lett 1978;16:205.
[26] Eckhardt H, Boudreaux DS, Chance RR. Effects of substituent-induced strain on the electronic-structure of polydiacetylenes. J Chem Phys 1986;85:4116.
[27] Olmsted J, Strand M. Fluorescence of polymerized diacetylene bilayer films. J Phys Chem-US 1983;87:4790.
[28] Haglund C, Lindgren J, Roberts PJ, Nordling S. Gastrointestinal cancer-associated antigen CA 19-9 in histological specimens of pancreatic tumours and pancreatitis. Br J Cancer 1986;53:189.
[29] Loy TS, Sharp SC, Andershock CJ, Craig SB. Distribution of CA 19-9 in adenocarcinomas and transitional cell carcinomas. An immunohistochemical study of 527 cases. Am J Clin Pathol 1993;99:726.
[30] Makovitzky J. The distribution and localization of the monoclonal antibody-defined antigen 19-9 (CA19-9) in chronic pancreatitis and pancreatic carcinoma. An immunohistochemical study. Virchows Arch B Cell Pathol Incl Mol Pathol 1986;51:535.
[31] Ohshio G, Ogawa K, Kudo H, et al. Immunohistochemical studies on the localization of cancer associated antigens DU-PAN-2 and CA19-9 in carcinomas of the digestive tract. J Gastroenterol Hepatol 1990;5:25.
[32] Ahlgren S, Wallberg H, Tran TA, et al. Targeting of HER2-expressing tumors with a site-specifically 99mTc-labeled recombinant affibody molecule, ZHER2:2395, with C-terminally engineered cysteine. J Nucl Med 2009;50:781.
[33] Co MS, Landolfi NF, Nagy JO, et al. Properties and pharmacokinetics of two humanized antibodies specific for L-selectin. Immunotechnology 1999;4:253.